ANALYTICAL AND NUMERICAL THERMAL ANALYSIS ON FRICTION STIR WELDING USING POLYGONAL TOOL PIN

STEPHEN LEON JOSEPH LEON[1]*, ALFRED FRANKLIN VARGHESE[2], JOSEPH MICHEL[2] AND GOPINATH GUNASEKARAN[2]

[1]*Department of Mechanical Engineering, Saveetha School of Engineering, Saveetha Institute of Medical and Technical Sciences, Chennai, Tamilnadu, India.*
[2]*Engineering Department, University of Technology and Applied Sciences-Ibri, Oman.*

*Corresponding author: stephenleonj@gmail.com

ABSTRACT: Frictional heat generation in the tool/matrix interface followed by the stirring of material along the weld line causes plasticized solid state joining in friction stir welding. In this paper, the existing torque based thermo-mechanical model for the tools with cylindrical pins is remodified for the polygonal tool pin profile by introducing novel multiplication factors with respect to the number of sides in the tool pin geometry. The variation in the effective heat supply with respect to the chosen pin geometry was analyzed. A comparative analysis of the proposed analytical model with the existing model was also carried out to understand the accuracy of the proposed model. Furthermore, a transient thermal numerical modelling was carried out in the view of understanding the change in process peak temperature in the stir zone and change in temperature gradient along the heat affected zone with respect to the change in pin geometry for the opted set of process input parameters. An analytically estimated heat-input-based numerical model was adopted in the present study. It was observed that the process peak temperature was directly proportional to the number of sides in the tool pin.

ABSTRAK: Penjanaan haba geseran antara muka pada alat/matrik diikuti dengan pengacauan material sepanjang garis kimpalan menyebabkan keadaan plastik pepejal melekat bersama geseran kimpalan pengacau. Kajian ini berkaitan tork sedia ada berdasarkan model mekanikal-terma bagi alat pin silinder yang terubah suai bagi profil pin alat poligon dengan memperkenalkan faktor gandaan berdasarkan bilangan sisi geometri alat pin. Perubahan pada bekalan haba efektif berdasarkan geometri pin pilihan telah dikaji. Analisis bandingan pada model analitik yang dicadang bersama model sedia ada, telah dilakukan bagi memahami ketepatan model cadangan. Tambahan, model transien numerikal terma telah dibuat bagi memahami proses perubahan suhu puncak ketika zon pengacauan dan perubahan gradien suhu sepanjang zon terkena haba perubahan geometri pin pada set proses parameter input terpilih. Kajian ini mengaplikasi model numerik berdasarkan input anggaran haba secara analitik. Dapatan kajian menunjukkan suhu puncak proses adalah berkadar langsung dengan bilangan sisi pin alat.

KEYWORDS: *thermal mode; friction stir welding; polygonal tool pin; transient model*

1. INTRODUCTION

The process peak temperature rise in friction stir welding during the welding stage is always maintained lower than the solidus temperature of the material to be joined so that this joining process can be considered as a solid-state metal joining technique. The major heat input for this solid-state welding technique is generated along the tool/matrix contact due to friction and it is assisted by the heat generation through the plastic deformation of material during the joining process under the tool shoulder [1]. The tool rotates and slides over the stationary workpiece, resulting in a relative velocity along the tool/matrix interface that is the root cause of the friction heat. This solid-state joining process is divided into different stages based on the position of the tool (Fig.1). Temperature gradient developed in the process at various distances from the axis of rotation of the tool is the key factor that decides the post weld mechanical properties of the joint [2].

Various software assisted simulations are used to estimate the influence of various internal and external factors of the heat generation. Shi et al. [4] studied temperature results through finite element analysis conducted using ABAQUS. Their thermo-mechanical analysis was validated through experimental results. A two-dimensional finite element model developed by Lockwood and Reynolds [5] for friction stir welding in aluminum alloy 2024-T351. The obtained temperature distribution from the FE model was validated by the experimental results.
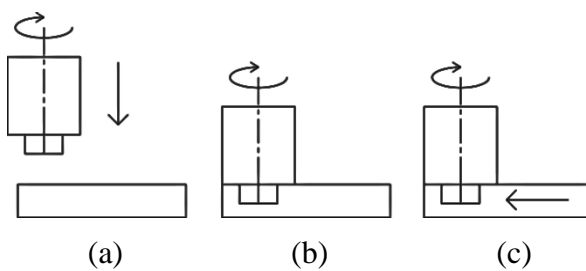

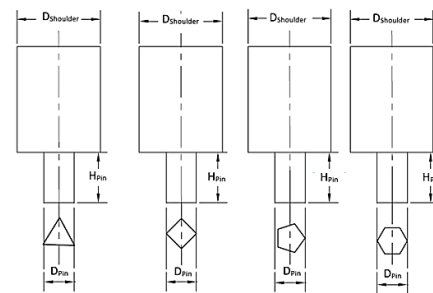Fig. 1: Stages in FSW: (a) plunging, (b) dwelling, (c) welding.

Fig. 2: Tools with polygonal tool pin.

Ullessy [2] evaluated the impact of variation in the tool speed on the thermal field by developing a three-dimensional viscoplastic model using computational fluid dynamics. A better simulation was obtained by Li et al. [6] using ABAQUS software for the fully sticking condition of tool-workpiece interface. Sanjeev et al. [7] analyzed the influence of the friction coefficient on the simulation output using ABAQUS and found that the coefficient of friction was equal to 1.0 during a sticking condition. Apart from similar material, little research was done to optimize process parameters on the joining of two dissimilar materials [8]. Labesh et al. [9] compared the effects of dwell time, tool speed, and plunge depth and found dwell period had higher influence on post weld joint strength over other factors.

In this solid-state welding, major amounts of effective heat supply are obtained along the interface of shoulder/matrix and a part of heat generated along the contact surface of the tool pin and material assists to maintain a constant temperature gradient along the stir zone. Analysis on the joint efficiency of the various welds developed on the usage of a tool with different non-circular straight pin profiles concluded that the tool with a square pin delivered a superior weld quality [10]. Better weld quality [11] was observed on a taper cylindrical pin profile compared to a square pin profile and it was concluded that the

increase in number of sides of a noncircular pin profile, from square profile to hexagon profile, increased the heat generation rate during welding. An experimental study [12] was carried out to understand the effects of tool pin geometries on the joint strength and it was found that tool pin geometry with square cross-sectional shape delivered a better weld quality than other polygonal shapes. Apart from these, various research [13-17] concluded that geometrical change in the tool pin geometry resulted in considerable changes in heat generation that in turn affected the temperature gradient during the joining process. So, tool pin geometry can also be a key factor with other parameters like tool feed rate and tool rotational speed. In this paper, for a given constant working condition, analytical expressions are derived and validated with the published results to analyze the quantity of heat supplied by the different polygonal pin profiles with the number of sides varying from three to six. Furthermore, heat generation during dwell, not only plasticizes the metal under the tool but also softens the neighboring material, which reduces the opposing forces to the tool movement [18]. This underlines the importance of analyzing the transient temperature increase during the dwell period. So, the effect of variation in tool pin geometry on the transient temperature gradient during the dwell period in the stir zone were compared through the results obtained from combined analytical and numerical approaches.

2. ANALYTICAL MODELLING

In the view of simplifying the analytical solution, the following assumptions were made: (i) Estimation of total torque developed during the process is the combined effect of friction along the contact surface and plastic deformation under the tool shoulder; (ii) The small quantity of heat developed during the initial stage (plunging) is neglected [19].
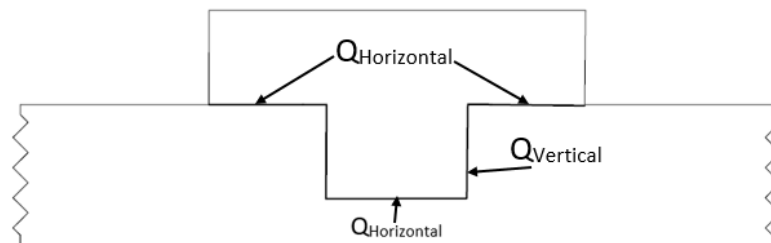

Fig 3: Tool/matrix frictional contact surfaces.

Total heat-generating surfaces are divided into horizontal and vertical surfaces as shown in Fig. 3. Frigaard et al. [20] estimated the total heat generation along the horizontal contact surface as,

$$Q_{\text{Horizontal}} = Q_{\text{Shoulder}} + Q_{\text{pin-tip}} = \frac{2}{3}\pi\sigma_{contact}\omega R_s^3$$

In the tool shoulder contact surface,

$$Q_{\text{Shoulder}} = \left[\frac{2}{3}\pi\sigma_{contact}\omega R_s^3\right] - Q_{\text{pin-tip}}$$

$$Q_{\text{Vertical}} = Q_{\text{Pin-side}}$$

For every tool pin geometry, the geometrical shape of the shoulder does not vary considerably. The uniform shoulder/matrix contact surface indicates that there will not be any change in heat generated by the tool shoulder irrespective of its pin geometrical shape. But there is a considerable change in tool pin contact surface area when the pin geometry varies.
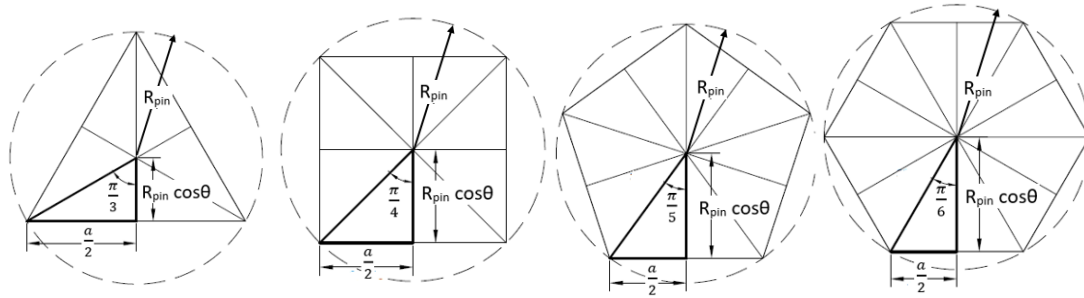
Fig. 4: Cross section of pin profiles and segments.

Polygonal tool pins shown for the current analysis were divided into small triangles as denoted in Fig. 4. The total amount of triangular divisions in every polygonal pin geometry was equal to two times the number of sides in the cross-sectional shape of the tool pin.

Schmidt et al. [21] estimated total torque developed in FSW as,

Rotating torque = $\sigma_c \, \omega \, x^2 \, d\theta \, dr$ (1)

where σ_c denotes contact stress, ω represents tool rotational speed, x is the distance of any point form the axis of rotation.

Considering one segment in Fig. 4,

$$Q_{pin-tip} = \iint \sigma_c \, \omega x^2 d\theta dx$$

$$D = f(x,\theta) \begin{cases} 0 \leq \theta \leq \dfrac{\pi}{z} \\ 0 \leq x \leq R_{pin} cos\theta \end{cases}$$

$$Q_{Pin\text{-}tip} = \sigma_c \omega \int_0^{\frac{\pi}{z}} d\theta \int_0^{R_{pin}cos\theta} f(x)dx$$

Torque developed for the entire pin can be obtained by,

Total torque developed = $\int_0^{\pi/z} \int_0^{R_{pin}cos\theta} \tau_c \, \omega \, x^2 \, d\theta \, dr$

$$= \sigma_c \, \omega \, R_{pin}^3 \left[\frac{1}{3} sin\theta - \frac{sin^3\theta}{9} \right]_0^{\pi/z} \tag{2}$$

For the tool pin/matrix horizontal contact surface,

$$Q_{pin\text{-}tip} = z \, \sigma_c \, \omega R_{pin}^3 \left[\frac{2}{3} \sin\left(\frac{\pi}{z}\right) - \frac{2sin^3\left(\frac{\pi}{z}\right)}{9} \right] \tag{3}$$

where z represents the sides in the chosen polygonal pin geometry.
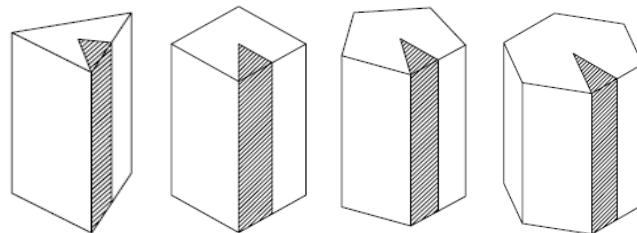

Fig. 5: Vertical surface segments.

Like the horizontal contact surface, the vertical contact surface can also be divided into small segments as denoted in Fig. 5. The quantity of rectangular divisions in each shape is equal to two times of the number of sides in the tool pin. For every rectangular vertical surface,

$$Q_{pin-vertical} = \iint \sigma_c \, \omega x^2 d\theta dx$$

$$D = f(x,\theta) \begin{cases} 0 \le \theta \le \frac{\pi}{z} \\ 0 \le x \le h \end{cases}$$

$$Q_{Pin\text{-}tip} = \sigma_c \omega \int_0^{\frac{\pi}{z}} d\theta \int_0^h f(x)dx$$

$$\text{Torque developed} = \int_0^{H_{pin}} \int_0^{(\frac{\pi}{z})} \sigma_c \, \omega R_{pin}^2 \, cos^2\theta d\theta \, dh$$

$$= \sigma_c \, \omega \, R_{pin}^2 \; H_{pin} \left[\frac{\pi}{2n} + \frac{1}{4} \sin(2\pi/z) \right] \tag{4}$$

For the pin vertical/matrix contact surface,

$$Q_{pin\text{-}vertical} = \frac{z}{2} \sigma_c \, \omega \, R_{pin}^2 \, H_{pin} \left[\frac{2\pi}{z} + \sin(2\pi/z) \right] \tag{5}$$

where, contact stress $\sigma_c = \mu P$, μ is the friction coefficient, ω is the angular velocity of the tool, pin height (H_{pin}) and shoulder radius (R_s) represent the dimensions of the pin. P is the vertical force given by the tool.

A standard method of prescribing tool pin dimension is through its side length. So the above derived equations have to be rearranged by side length (a). The relationship between pin circumferential radius and pin side length can be represented as,

$$R_{pin} = \frac{a}{2Sin\left(\frac{\pi}{z}\right)} \tag{6}$$

Applying this, equations (3 – 5) can be remodified as,

$$Q_{pin\text{-}tip} = n \, \sigma_c \, \omega \, \frac{a^3}{8Sin^3\left(\frac{\pi}{n}\right)} \left[\frac{2}{3} \sin\left(\frac{\pi}{z}\right) - \frac{2sin^3\left(\frac{\pi}{z}\right)}{9} \right] \tag{7}$$

$$Q_{pin\text{-}tip} = \frac{1}{12} z \, \sigma_c \, \omega \, a^3 \left[\frac{1}{Sin^2\left(\frac{\pi}{z}\right)} - \frac{1}{3} \right] \tag{8}$$

$$Q_{pin\text{-}vertical} = z \, \sigma_c \, \omega \frac{a^2}{8Sin^2\left(\frac{\pi}{z}\right)} \, H_{pin} \left[\frac{2\pi}{z} + \sin\left(\frac{2\pi}{z}\right) \right] \tag{9}$$

$$Q_{pin\text{-}vertical} = z \, \sigma_c \, \omega \, a^2 H_{pin} \left[\frac{\pi}{4Sin^2\left(\frac{\pi}{z}\right)} - \frac{1}{4} \frac{cos\left(\frac{\pi}{z}\right)}{sin\left(\frac{\pi}{z}\right)} \right] \tag{10}$$

$$Q_{pin\text{-}vertical} = z \, \sigma_c \, \omega \, a^2 H_{pin} \left[\frac{\pi}{4Sin^2\left(\frac{\pi}{z}\right)} - \frac{1}{4tan\left(\frac{\pi}{z}\right)} \right] \tag{11}$$

These equations can be simplified by introducing multiplication factors as,

$$Q_{pin\text{-}tip} = X_R \, \tau_c \, \omega \, R_{pin}^3 \tag{12}$$

$$Q_{pin\text{-}vertical} = Y_R \; \tau_c \, \omega \, R_{pin}^2 \, H_{pin} \tag{13}$$

$$Q_{pin\text{-}tip} = X_S \, \tau_c \, \omega \, a^3 \tag{14}$$

$$Q_{pin\text{-}vertical} = Y_S \, \tau_c \, \omega \, a^2 H_{pin} \tag{15}$$

The values of multiplication factors for various number of pin sides are given in Table 1.

Table 1: Multiplication factor values

Pin shape	X_R Value	Y_R Value	X_S Value	Y_S Value
Triangular (n=3)	1.33	4.50	0.27	3.40
Square (n=4)	1.54	5.01	0.64	7.15
Pentagonal (n=5)	1.72	5.44	1.25	12.72
Hexagonal (n=6)	1.89	5.82	2.16	20.35

Based on the obtained values for the given number of sides, these multiplication factors can be written as a function of number of sides (z),

$$X_R = 0.77z^{0.5} \tag{16}$$

$$Y_R = 3z^{0.37} \tag{17}$$

$$X_s = 0.01z^3 \tag{18}$$

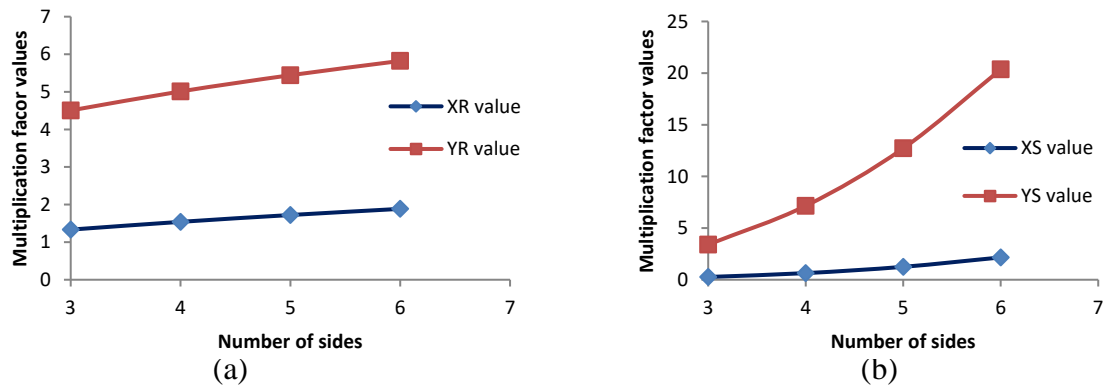$$Y_s = 0.2z^{2.58} \tag{19}$$

Fig. 6: Change in multiplication values (X_R and Y_R) (a) when radius of pin is considered, (b) when pin side length is considered.

3. NUMERICAL MODELLING

In ANSYS workbench, transient temperature rises for different pin profiles, Triangular(T), Square (S), Pentagonal (P) and Hexagonal (H)) were analyzed using analytically estimated heat input for different pin profiles to analyze variation in dwell period to reach the required peak temperature in order to switch over from dwell period to weld period. Applied heat flux does not change in the X and Z directions and it varies only with respect to the Y direction as the thermal conductivity reduces heat flow towards the depth of the workpiece. So, a two-dimensional cross section geometry model was adopted for the analysis. A AA2024-T3 plate was considered as the base material for the current analysis. Other properties considered for the analysis are denoted in Tables 2 and 3.

Table 2: Temperature dependent thermal property of base metal [15]

Temperature (K)	290	373	473	573	673
Specific heat capacity (J kg^{-1} K^{-1})	864	921	1047	1130	1172
Thermal conductivity (W m^{-1} K^{-1})	120	134.4	151.2	172.2	176.4

Table 3: process parameters and tool material properties

Property/parameter	Value
Diameter of tool shoulder (mm)	15
Diameter of the pin (mm)	5
Height of the tool pin (mm)	5.7
Base metal thickness (mm)	6
Material density (tool) (kg/m^3)	7930
Density of base metal (kg/m^3)	2780
Tool specific heat capacity (J kg^{-1} K^{-1})	502
Thermal conductivity of tool (W m^{-1} K^{-1})	21.4
Base metal bottom side heat transfer coefficient at the bottom of the workpiece (W m^{-2} K^{-1})	300
Base metal top side Heat transfer coefficient (W m^{-2} K^{-1})	50
Base metal other side heat transfer coefficient (W m^{-2} K^{-1}) except top and bottom surfaces	200

3.1 Boundary and Initial Conditions

At tool shoulder/matrix interface

$$k\left(\frac{\partial T}{\partial n}\bigg|_{sholder}\right) = \eta(Q_{horizontal} - Q_{pin\text{-}tip}) \bigg|_{\substack{R_{pin} \leq X \leq R_s \\ t > 0}}$$

At Pin tip/matrix interface

$$k\left(\frac{\partial T}{\partial n}\bigg|_{Pin-tip}\right) = \eta \, Q_{pin\text{-}tip} \bigg|_{\substack{0 \leq X \leq R_{pin} \\ t > 0}}$$

At Pin vertical/matrix interface

$$k\left(\frac{\partial T}{\partial n}\bigg|_{Piin-vertical}\right) = \eta \, Q_{pin\text{-}vertical} \bigg|_{\substack{0 \leq Y \leq H_{pin} \\ t > 0}}$$

Convective heat transfer from other surfaces to atmosphere

$$k\left(\frac{\partial T}{\partial n}\bigg|_{Top-bottom-side}\right) = h_x \, (T_x - T_{amb}),$$

where h_x represents convective heat transfer coefficient between base metal and atmosphere, T_x is surface temperature of the workpiece during the joining process at different points and T_{amb} refers to ambient temperature. For the model simplicity, the bottom surface is also considered to be directly in contact with ambient air.

Here, η refers to the percentage of heat transferred to the workpiece. For the current analysis it had been considered as 95%, with the remaining 5% transferred through the tool.
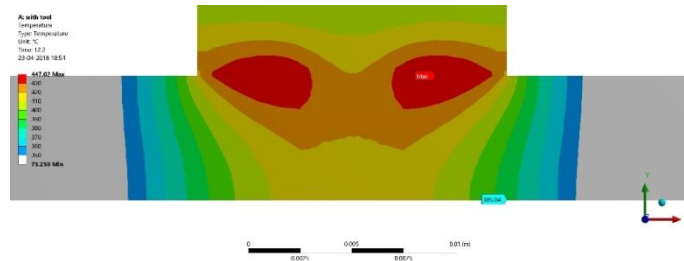
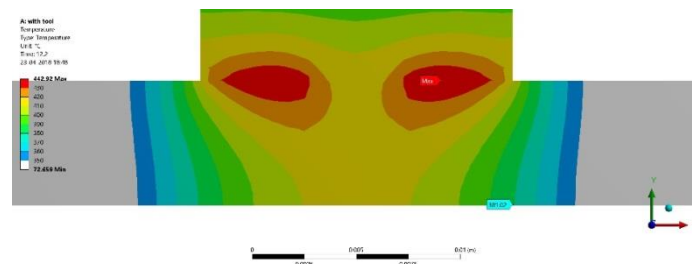$$T(x,y) = T_{initial} = 22 \text{ °C at any point when time } t > 0$$
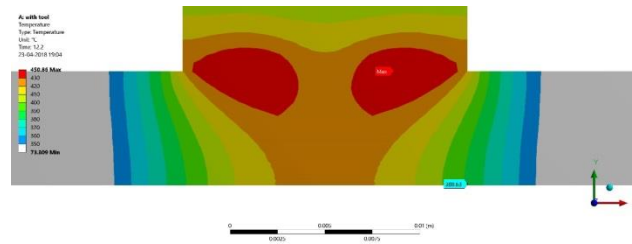
(a) Thermal distribution when hexagonal shaped pin is used.
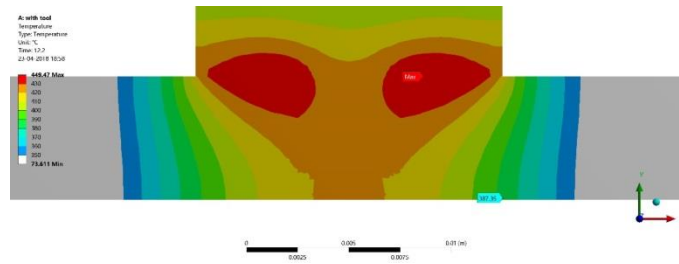
(b) Thermal distribution when pentagonal shaped pin is used.

(c) Thermal distribution when square shaped pin is used.

(d) Thermal distribution when triangular shaped pin is used.

Fig. 7: Temperature distribution with different pin shapes used at 12.2 s of dwell period.

4. RESULTS AND DISCUSSION

For the current analysis dwell period is considered as the time required to reach a peak temperature of 90% of the melting temperature (775 K) of AA2024-T3. Length of the pin side for different pin geometries (C, S, P and H) were selected in such a way that their pin radius remains constant. In the view of validation of the obtained transient model, the estimated amount of effective heat supply during different process conditions is compared with an analytical model developed by Gadakh et al. [15],

$$Q_{Total} = \frac{2}{3}\pi\tau_{contact}\omega(R_s^3 + X.R_{pin}^2 H_{pin}) \tag{20}$$

where multiplication factor X varies from 0.72 to 3 for different pin profiles.

Comparative analysis of heat generated along the different contact surfaces of the tool with the base metal are denoted in the Table.4.

Table 4: Total heat generation at by the different pin profiles

Pin profile	$Q_{Shoulder}$ (kW)	$Q_{Pin-tip}$ (kW)	$Q_{Pin-Vertical}$ (kW)	Q_{total} (kW)	Q_{total} (kW) Gadhakh et al. [15]
Triangular	4335.55	94.2	397.33	4827.09	4699.08
Square	4306.51	123.24	458.18	4887.94	4785.11
Pentagon	4293.69	136.06	492.19	4921.95	4874.89
Hexagon	4288.45	141.3	510.09	4939.84	4964.67

Gahakh et al. [15] obtained a heat generation model [Eq. 22] based on the assumption that any tool pin shape occupies a circular contact area when it rotates. While obtaining the effective heat supply along the tool horizontal surface ($Q_{shoulder}$ + $Q_{pin-tip}$), this assumption was justified as the combined geometry of the horizontal surface of tool shoulder and pin occupies a circular contact shape. But while obtaining the heat generation values separately for shoulder/matrix, tool pin tip/matrix, tool side/matrix interfaces, it did not show any variation in the effective heat supply by the horizontal tool contact surfaces of all pin shapes and variations were absorbed along the vertical contact surface of the tool pin.
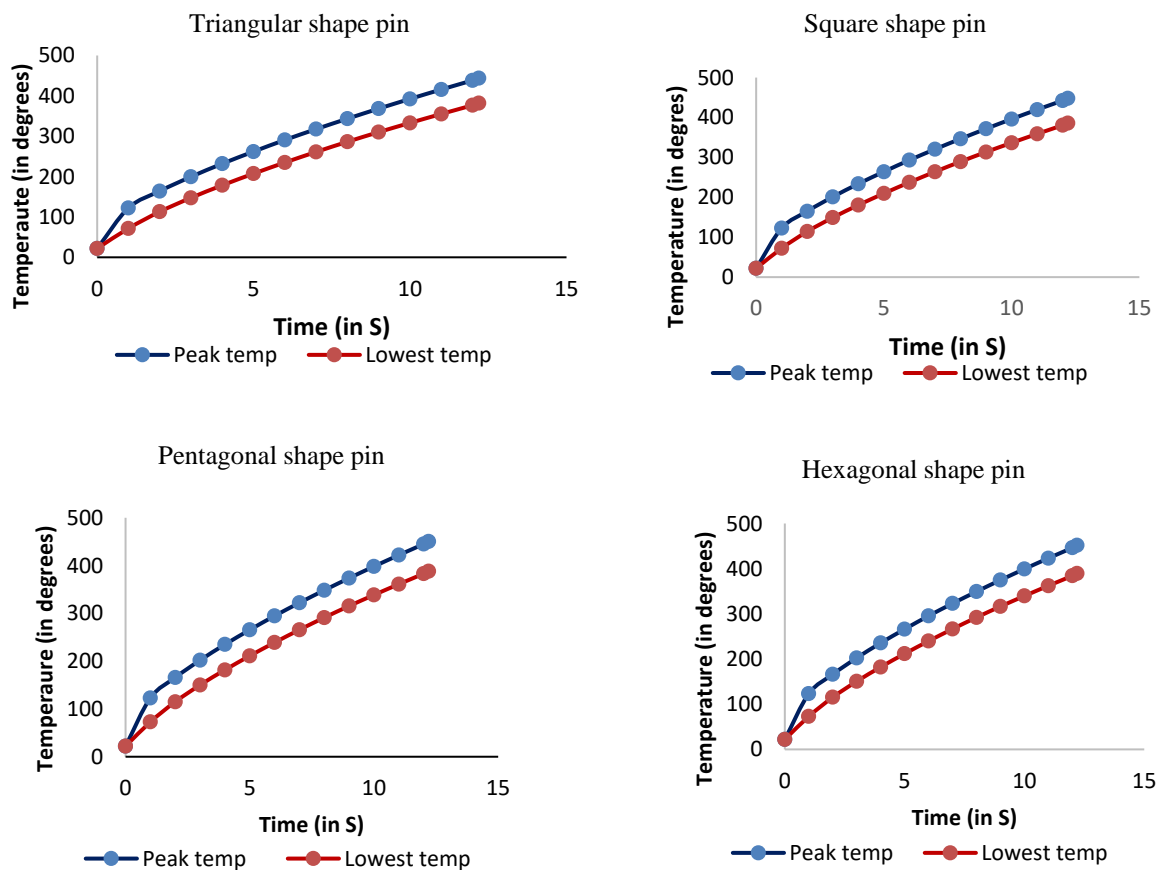

Fig. 8: Transient temperature rises for different pin profiles.

Although the tool pin occupies a circular area irrespective of pin shape while rotating, at any instance of time, contact surface cannot be circular and it varies with

respect to the number of sides considered. As in the derived equations (Eq. 14, 15, 16 & 17) the exact geometry of the tool pin was considered, the accuracy of the obtained result was improved. It can be noticed from Table 4. that the estimated heat generation by the horizontal surface varies with the increase in tool pin sides.

From Fig. 9 it can be observed that the time taken to attain process peak temperature by the hexagonal pin profile is low compared to other shapes and time required increases when the number of sides decreases from pentagonal shape to triangular shape as the heat generated by the contact surface decreases.

Transient temperature rise in a point where the minimum temperature was absorbed in the stir zone is also denoted in Fig. 8. For a constant input rotational speed, maximum and minimum temperatures were observed at different points along the stir zone and shown in Fig. 8 to analyze the temperature gradient at an instance of time. Rapid peak temperature achievement of the hexagonal pin profiled tool reveals the high intensity of effective heat input by the vertical pin surface which assists in quick plasticization of the nearby layer. Isolines obtained from the numerical modelling (Fig. 7) explain the relationship between the intensity of heat supplied and the variation of thermal field along the stir zone for an instance of time. The increase in the number of tool pin sides increases the temperature gradient in the material flow zone at the given instance of time.

The purpose of the dwell period is to increase the temperature of the material under the tool shoulder until it plasticizes in order to reduce flow stress to obtain a high rate of strain around the tool pin. Plasticized material not only has less flow stress but also has lower strength to resist the movement of the tool during the weld, which increases tool life. Increase in the heat intensity reduces the ideal dwell period and increases the welding speed [22]. Increase in welding speed in turn reduces the heat affected zone. As a result, it is understood that an increase in the tool pin sides results in an increase in energy input which drastically decreases temperature rise in the heat affected zone. Failure in FSW joints often occurs in the heat affected zone due to the existence of fewer needle-shaped precipitates. When the effective heat supply intensity is increased, tool feed rate can be increased. When the tool feed rate increased, the heat affected zone is reduced and the temperature gradient in the stir zone also becomes uniform around the tool pin, which in turn reduces the residual stress in the joints.
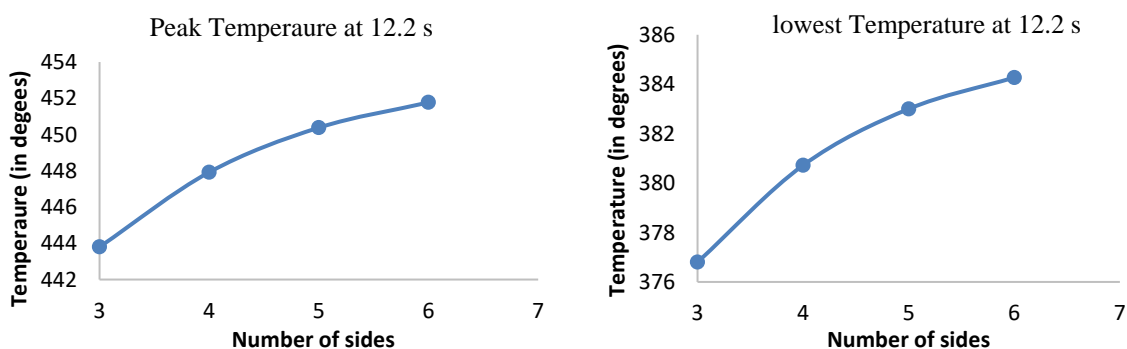
Fig. 9: Change in peak and low temperatures in the stir zone.

Obtained results indicate that although the vertical surface has a limited contribution on total heat supply, it has a major influence on the distribution of heat along the stir zone during the joining process in friction stir welding. From the graph (Fig. 9) it is evident that

increase in the number of tool pin sides, increases the percentage contribution of the vertical surface in the total heat generation.

5. CONCLUSIONS

A novel heat generation model was derived and validated with the goal of analyzing the change in the effective heat supply according to the geometrical changes in tool pin. From the analytical and numerical study on the thermal field developed during the joining process, it can be concluded that:

- Numerical analysis on transient temperature increase during the process suggests that the dwell time is directly proportional to the tool pin sides in the polygonal shape. The increase in tool pin sides has considerable effect on the temperature rise along the heat affected zone.

- Process peak temperature increases with the increase in tool pin sides. A maximum of 452 ºC is absorbed for the hexagonal pin geometry and a minimum of 443.6 ºC is observed for the triangular tool pin geometry.

- For hexagonal tool pin geometry, the effective heat supply intensity is high, which facilities increase in tool feed rate. When the tool feed rate increased, the heat affected zone is reduced and the temperature gradient in the stir zone is also maintained uniform around the tool pin, which in turn reduces the residual stress in the joints.

- From the analytical heat generation estimation, it was understood that the increase in the number of sides in the tool pin increases the percentage contribution of the tool pin on the effective heat supply during the process. For the given process input conditions, usage of the hexagonal tool pin increases the total quantity of heat input up to 330 J/s compared to the heat supply by the tool with the triangular shaped tool pin.

REFERENCES

[1]   Leon JS, Jayakumar V. (2019) An investigation of analytical modelling of friction stir welding. Int. J. Mech. Prod. Eng. Res. Dev., 9(1): 179-189.
      doi: 10.24247/ijmperdfeb201918.
[2]   Ulysse P. (2022) Three-dimensional modeling of the friction stir welding process. Int. J. Mach. Tools. Manuf., 42: 1549–1557.
[3]   Shi Q, Dickerson T, Shercliff HR. (2003) Thermo-mechanical FE modelling of friction stir welding of Al-2024 including tool loads, 4th International Symposium on Friction Stir Welding, Park City, Utah, USA, 14-16 May 2003.
[4]   Lockwood WD, Reynolds AP. (2003) Simulation of the global response of a friction stir weld using local constitutive behavior. Materials Science and Engineering, A339: 35-42.
[5]   Li W, Shi S, Wang F, Zhang Z, Ma T, Li J. (2012) Numerical simulation of friction welding processes based on ABAQUS environment. J. Eng. Sci. Tech. Rev., 5: 10-19.
[6]   Sanjeev NK, Vinayak M, Suresh Hebbar H. (2014) Effect of coefficient of friction in finite element modeling of friction stir welding and its importance in manufacturing process modelling applications. Int. J. Appl. Sci. Eng. Res., 3: 755-762.
[7]   Palanivel R, Mathews PK, Murugan N, Dinaharan I. (2012) Effect of tool rotational speed and pin profile on microstructure and tensile strength of dissimilar friction stir welded AA5083-H111 and AA6351-T6 aluminium alloys. Mater. Des., 40: 7-16.

[8]   Labesh Kumar C, Jayakumar V, Bharathiraja G. (2020) Optimization of welding parameters for friction stir spot welding of AA6062with similar and dissimilar thicknesses. Materials Today: Proceedings.   https://doi.org/10.1016/j.matpr.2019.07.204.

[9]   Labesh Kumar C, Jayakumar V, Bharathiraja G. (2019) Optimisation of friction stir spot welding parameters of AA6062-ST1020 lap joint. Int. J. Mech. Prod. Eng. Res. Dev., 3: 10727-10732.

[10] Suresha CN, Rajaprakash BM, Upadhya S. (2011) A study of the effect of tool pin profiles on tensile strength of welded joints produced using friction stir welding process. Mater. Manuf., 26(9): 1111-1116.

[11] Fujii H, Cui L, Maeda M, Nogi K. (2006) Effect of tool shape on mechanical properties and microstructure of friction stir welded aluminium alloys. Mater. Sci. Eng., 419: 25-31.

[12] Stephen Leon J, Bharathiraja G, Jayakumar V. (2021) Experimental analysis on friction stir welding using flat-faced Pins in AA2024-T3 Plate. FME Transactions, 49: 78-86. doi: 10.5937/fme2101078S.

[13] Vijay SJ, Murugan N. (2010) Influence of tool pin profile on the metallurgical and mechanical properties of friction stir welded Al–10 wt.% TiB2 metal matrix composite. Mater. Des., 31: 3585-3589.

[14] Leon SJ, Bharathiraja G, Jayakumar V. (2020) Durability map for the friction stir welding tools with flat faced Pins. Int J of Integrated Engineering, 2(8): 83-96 doi: 10.30880/ijie.2020.12.08.008.

[15] Gadakh VS, Kumar A. (2014) Friction stir welding window for AA6061-T6 aluminium alloy. Proc IMechE, Part B: J Engineering Manufacture, 228(9): 1172-1181.

[16] Stephen Leon J, Bharathiraja G, Jayakumar V. (2020) Analytical and experimental investigations of optimum thermomechanical conditions to use tools with non-circular pin in friction stir welding. Int. J. Adv. Manuf. Technol., 107: 11-12. doi: 10.1007/s00170-020-05341-7.

[17] Shi L, Wu CS. (2017) Transient model of heat transfer and material flow at different stages of friction stir process. J. Manuf. Proc., 25: 323-339.

[18] Hamilton C, Dymek S, Sommers A. (2008) A thermal model of friction stir welding in aluminium alloys. Int J Mach Tools & Manuf., 48(10): 1120-1130.

[19] Schmidt H, Hattel J. (2005) Modelling heat flow around tool probe in friction stir welding. Sci Tech Weld Join, 10: 176-186.

[20] Frigaard O, Grong O, Midling OT. (2001) A process model for friction stir welding of age hardening aluminum alloys. Metall Mater Trans, 32(5): 1189-1200.

[21] Nandan R, DebRoy T, Bhadeshia HKDH. (2008) Recent advances in friction-stir welding – Process, weldment structure and properties. Prog Mater Sci, 53(6): 980-1023.

[22] Leon JS, Jayakumar V. (2020) Transient heat input model for friction stir welding using non-circular tool pin. FME Transactions, 48(1): 137-142. doi: 10.5937/fmet2001137L.